Національна академія наук України

ІНСТИТУТ ФІЗИКИ КОНДЕНСОВАНИХ СИСТЕМ

ICMP–24–02E

T. Hutak, T. Krokhmalskii, J. Schnack[*], J. Richter[†], O. Derzhko

THERMODYNAMICS OF THE $S = 1/2$ HYPERKAGOME-LATTICE HEISENBERG ANTIFERROMAGNET

[*]Fakultät für Physik, Universität Bielefeld, Postfach 100131, 33501 Bielefeld, Germany

[†]Institut für Physik, Otto-von-Guericke-Universität Magdeburg, P.O. Box 4120, 39016 Magdeburg, Germany

ЛЬВІВ

УДК: 537.9; 537.622

PACS: 75.10.Jm

Термодинаміка $S = 1/2$ антиферомагнетика Гайзенберга на гратці гіперкагоме

Т. Гутак, Т. Крохмальський, Ю. Шнак, Й. Ріхтер, О. Держко

Анотація. Використано 16 доданків високотемпературного розвинення для S=1/2 антиферомагнетика Гайзенберга на гратці гіперкагоме, доповнених методом ентропії, щоб дослідити теплоємність c і однорідну сприйнятливість χ моделі. Розглянуто два сценарії: безщілинний чи щілинний енергетичний спектр. c, крім піку поблизу $T\approx$0.669, має низькотемпературний пік при $T\approx$0.021−0.033. Вигляд χ нижче T=0.5 сильно залежить від вибраного сценарію. Енергія основного стану – $e_0 \in [-0.440, -0.435]$. Обчислено c і χ для скінчених граток з N=24 і 36 вузлів. Результати свідчать на користь безщілинного сценарію, коли максимум χ при $T\approx$0.118−0.194 краще погоджується в обох методах.

Thermodynamics of the $S = 1/2$ hyperkagome-lattice Heisenberg antiferromagnet

T. Hutak, T. Krokhmalskii, J. Schnack, J. Richter, O. Derzhko

Abstract. The S=1/2 hyperkagome-lattice Heisenberg antiferromagnet allows to study the interplay of geometrical frustration and quantum as well as thermal fluctuations in three dimensions. We use 16 terms of a high-temperature series expansion complemented by the entropy-method interpolation to examine the specific heat and the uniform susceptibility of the S=1/2 hyperkagome-lattice Heisenberg antiferromagnet. We obtain thermodynamic quantities for the two possible scenarios of either a gapless or a gapped energy spectrum. We have found that the specific heat c exhibits, besides the high-temperature peak around $T\approx$0.669, a low-temperature one at $T\approx$0.021−0.033. The functional form of the uniform susceptibility χ below about T=0.5 depends strongly on whether the energy spectrum is gapless or gapped. The value of the ground-state energy can be estimated to $e_0 \in [-0.440, -0.435]$. In addition to the entropy-method interpolation we use the finite-temperature Lanczos method to calculate c and χ for finite lattices of N=24 and 36 sites. A combined view on both methods leads us to favour a gapless scenario since then the maximum of the susceptibility at $T\approx$0.118−0.194 agrees better between both methods.

Подається в Physical Review B

Submitted to Physical Review B

Препринти Інституту фізики конденсованих систем НАН України розповсюджуються серед наукових та інформаційних установ. Вони також доступні по електронній комп'ютерній мережі на WWW-сервері інституту за адресою http://www.icmp.lviv.ua/

The preprints of the Institute for Condensed Matter Physics of the National Academy of Sciences of Ukraine are distributed to scientific and informational institutions. They also are available by computer network from Institute's WWW server (http://www.icmp.lviv.ua/)

Тарас Ігорович Гутак
Тарас Євстахійович Крохмальський
Юрген Шнак
Йоганес Ріхтер
Олег Володимирович Держко

Термодинаміка $S = 1/2$ антиферомагнетика Гайзенберга на гратці гіперкагоме

Роботу отримано 5 серпня 2024 р.

Затверджено до друку Вченою радою ІФКС НАН України

Рекомендовано до друку відділом квантової статистики

Виготовлено при ІФКС НАН України

1. Introduction

Frustrated quantum spin systems are a subject of intense ongoing research in the field of magnetism [1–4]. Geometric frustration and quantum fluctuations may evade any ground-state ordering even in three dimensions. Among several famous examples, the $S = 1/2$ pyrochlore-lattice Heisenberg antiferromagnet has attracted much attention, being for decades a candidate for the realization of a spin-liquid state in three dimensions [5]. After intense numerical studies, a lattice symmetry breaking in the ground state has been revealed [6–9].

A closely related example is the $S = 1/2$ hyperkagome-lattice Heisenberg antiferromagnet. Inspired by experiments on the spinel oxide $Na_4Ir_3O_8$ [10], in which low spin d^5 Ir^{4+} ions reside on the vertices of a hyperkagome lattice, several theoretical studies for the classical ($S \to \infty$) and quantum ($S = 1/2$) Heisenberg antiferromagnet on such a lattice have been performed [11–19]. The main focus of these studies is at ground-state properties of the $S = 1/2$ hyperkagome-lattice Heisenberg antiferromagnet. For the ground state of this model a gapped quantum spin liquid with topological order [12] and a gapless quantum spin liquid with spinon Fermi surfaces [15] were proposed by Lawler *et al.*. In contrast, Bergholtz *et al.* [16] proposed a valence bond crystal with a 72 site unit cell as the ground state of this model; this implies a spin gap with a huge number of singlet excitations below the lowest triplet state and thus a power law for the specific heat and a vanishing susceptibility for vanishing temperature.

The finite-temperature properties of the $S = 1/2$ hyperkagome-lattice Heisenberg antiferromagnet have also been considered [15–17, 19]. It was argued that $c(T) \propto T^2$ at low T [15] (similar to what is observed for $Na_4Ir_3O_8$ [10]) and that $\chi(T)$ has a non-zero value at $T = 0$ and almost no temperature dependence as $T \to 0$ [19] (again in agreement with experimental data for $Na_4Ir_3O_8$ [10]). In addition, high-temperature series expansions for c and χ were developed and compared with the experimental data for $Na_4Ir_3O_8$ [17].

On the experimental side, apart from the mentioned iridate compound $Na_4Ir_3O_8$ [10], there are other solid-state realizations of the hyperkagome-lattice Heisenberg anitiferromagnet, see, e.g., Refs. [20–22]. Note, however, that the $5d$-based transition-metal oxides, such as $Na_4Ir_3O_8$, are known for having a large spin-orbit coupling so that the pure Heisenberg Hamiltonian apparently should be accomplished by other terms relevant for such materials [23]. Indeed, previous theoretical papers [15, 17, 19] compare $c(T)$ or $c(T)/T$ and $\chi(T)$ or $1/\chi(T)$

to available experimental data for the $S = 1/2$ hyperkagome antiferromagnet $Na_4Ir_3O_8$ [10]. These comparisons exhibit noticeable discreapancies roughly below $J/2$ (J is about 300 K for $Na_4Ir_3O_8$) and even at higher temperatures for the specific heat. The authors attributed this disagreement to an incomplete subtraction of nonmagnetic contribution to the experimentally measured $c(T)$ [17] and an insufficiency of the spin-isotropic Heisenberg model for description of the $S = 1/2$ hyperkagome antiferromagnet $Na_4Ir_3O_8$ [16, 23].

In the present paper, we consider the $S = 1/2$ hyperkagome-lattice Heisenberg antiferromagnet – a benchmark model of frustrated quantum magnets, and study its thermodynamics. The toolbox to tackle thermodynamics of frustrated quantum spin systems is rather scarce. Quantum Monte Carlo suffers from the sign problem [24], exact diagonalization or finite-temperature Lanczos methods are restricted to too small lattices [25–27], the density-matrix renormalization group technique requires a mapping via a "snake" path to a one-dimensional system [28]. Besides, the pseudofermion functional renormalization group approach focuses on the wave-vector-dependent susceptibility [19], whereas one more universal method, the rotation-invariant Green's function method [29–35], has not been applied to the $S = 1/2$ hyperkagome-lattice Heisenberg antiferromagnet so far.

In our study, we use the high-temperature series expansions to the order of β^{16} ($\beta = 1/T$) provided by Singh and Oitmaa in Ref. [17]. Singh and Oitmaa used the high-temperature series to compute various thermodynamic properties down to a temperature[1] of about $T \approx 0.25$ [17]. However, this range can be extended down to zero temperature if one combines the series expansion with possible assumptions about the low-energy spectrum of the spin model within the framework of the so-called "entropy method". The entropy-method interpolation of high-temperature series expansions was suggested by Bernu and Misguish [36] and later used in several studies [37–44]. In the present paper, we use the series expansion [17] and the entropy method [36, 38, 40, 41, 43] to obtain the temperature dependence for the specific heat $c(T)$ and the uniform susceptibility $\chi(T)$ for the $S = 1/2$ hyperkagome-lattice Heisenberg antiferromagnet. We also obtain a prediction for the ground-state energy of the model e_0, which provides self-consistency of the entropy-method calculations. Our entropy-method calculations are accompanied by finite-temperature Lanczos calculations for finite lattices up to 36 sites.

[1] Temperatures are given as multiples of the exchange interaction. $T = 0.25$ thus means $k_B T/J = 0.25$.

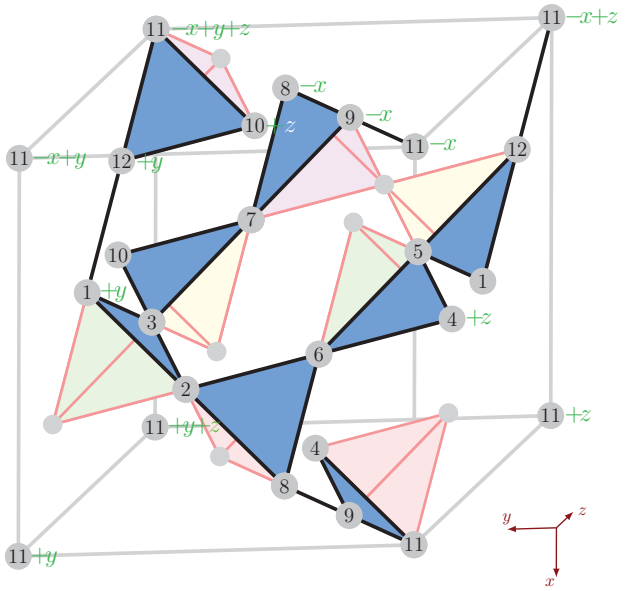

Figure 1. The hyperkagome lattice. Besides the 12 sites from the same unit cell ($1, \ldots, 12$ stand for $\boldsymbol{r}_1, \ldots, \boldsymbol{r}_{12}$), we show 13 more sites of the nearby unit cells (we use, e.g., $11 - x + y + z$ for $\boldsymbol{r}_{11} - \boldsymbol{e}_x + \boldsymbol{e}_y + \boldsymbol{e}_z$ to lighten notations). Additionally, we show 28 bonds (black lines); 15 bonds connect the sites from the same unit cell and 9 bonds connect the sites of the neighboring cells. The remaining 4 bonds, which connect the sites $1 + y$ and $12 + y$, $8 - x$ and $9 - x$, $9 - x$ and $11 - x$, $11 - x + y + z$ and $12 + y$, are shown for better clarity. We also display the underlying pyrochlore lattice.

The remainder of this paper is organized as follows. In Section 2 we introduce the model and briefly explain the methods to be used for obtaining the thermodynamic quantities. Then, in Section 3, we report our results for the ground-state energy e_0, the specific heat $c(T)$, and the uniform susceptibility $\chi(T)$. Finally, we discuss our findings in Section 4.

2. Model and methods

The hyperkagome lattice has been described in several papers. It can be viewed as a three-dimensional network of corner-sharing triangles with 12 sites in a cubic unit cell. It also can be viewed as a 1/4 depleted

pyrochlore lattice, meaning that three out of the four sites in every tetrahedron are occupied by spins. As a result, each spin of the three-dimensional hyperkagome lattice has only four nearest neighbors just as for the two-dimensional kagome lattice. There are several different conventions regarding the coordinates of lattice sites (see, e.g., Refs. [23, 45–47]). According to Fig. 1, we define the sites on the hyperkagome lattice sites by $\boldsymbol{R}_{\boldsymbol{n}\alpha} = \boldsymbol{R}_{\boldsymbol{n}} + \boldsymbol{r}_\alpha$. Here, $\boldsymbol{R}_{\boldsymbol{n}} = n_x\boldsymbol{e}_x + n_y\boldsymbol{e}_y + n_z\boldsymbol{e}_z$, where n_x, n_y, n_z are integers and $\boldsymbol{e}_x = (1,0,0)$, $\boldsymbol{e}_y = (0,1,0)$, $\boldsymbol{e}_z = (0,0,1)$, generates a simple cubic lattice. Moreover, the origins of the 12 equivalent sites in the unit cell may be defined by $\boldsymbol{r}_\alpha$, $\alpha = 1,\ldots,12$ with

$$\begin{aligned}
\boldsymbol{r}_1&=\frac{1}{4}\,(-2,0,2)\,,\boldsymbol{r}_2=\frac{1}{4}\,(-1,3,2)\,,\boldsymbol{r}_3=\frac{1}{4}\,(-2,3,1)\,,\\
\boldsymbol{r}_4&=\frac{1}{4}\,(-1,1,0)\,,\boldsymbol{r}_5=\frac{1}{4}\,(-2,1,3)\,,\boldsymbol{r}_6=\frac{1}{4}\,(-1,2,3)\,,\\
\boldsymbol{r}_7&=\frac{1}{4}\,(-3,2,1)\,,\boldsymbol{r}_8=\frac{1}{4}\,(0,2,2)\,,\boldsymbol{r}_9=\frac{1}{4}\,(0,1,1)\,,\\
\boldsymbol{r}_{10}&=\frac{1}{4}\,(-3,3,0)\,,\boldsymbol{r}_{11}=(0,0,0)\,,\boldsymbol{r}_{12}=\frac{1}{4}\,(-3,0,3)\,.
\end{aligned} \tag{1}$$

In Fig. 1, we denote $\boldsymbol{r}_1,\ldots,\boldsymbol{r}_{12}$ by $1,\ldots,12$. In addition, we display 13 sites of the nearby unit cells by $11-x+y+z$, $11-x+z$, $8-x$ and so on, where, e.g., $11-x+y+z$ means $\boldsymbol{r}_{11}-\boldsymbol{e}_x+\boldsymbol{e}_y+\boldsymbol{e}_z$, and so on.

In the present paper, we study a benchmark model in the theory of frustrated quantum magnetism and consider the isotropic Heisenberg Hamiltonian on the hyperkagome lattice, which is given by

$$H = J \sum_{\langle \boldsymbol{m}\alpha;\boldsymbol{n}\beta\rangle} \boldsymbol{S}_{\boldsymbol{m}\alpha}\cdot\boldsymbol{S}_{\boldsymbol{n}\beta}\,. \tag{2}$$

Here, we set the antiferromagnetic interaction $J = 1$, the sum runs over the nearest-neighbor bonds of the hyperkagome lattice, and $\boldsymbol{S}_{\boldsymbol{m}\alpha}$ represents the $S = 1/2$ spin-vector operator at the lattice site $\boldsymbol{R}_{\boldsymbol{m}\alpha}$. Expanding the sum in Eq. (2) for fixed $\boldsymbol{m}$, one gets 24 bonds, that is, 15 bonds connecting the sites within the unit cell with the same cell index $\boldsymbol{m}$ and 9 bonds connecting the sites of the unit cell $\boldsymbol{m}$ with the sites of the neighboring unit cells $\boldsymbol{m}-\boldsymbol{e}_x$, $\boldsymbol{m}-\boldsymbol{e}_y$, $\boldsymbol{m}-\boldsymbol{e}_z$, $\boldsymbol{m}-\boldsymbol{e}_x+\boldsymbol{e}_y$, $\boldsymbol{m}+\boldsymbol{e}_x-\boldsymbol{e}_z$, and $\boldsymbol{m}+\boldsymbol{e}_y-\boldsymbol{e}_z$, see Fig. 1. The remaining 4 bonds in Fig. 1, i.e., the ones which connect the sites $1+y$ and $12+y$, $8-x$ and $9-x$, $9-x$ and $11-x$, $11-x+y+z$ and $12+y$ (cf. the bonds connecting the sites 1 and 12, 8 and 9, 9 and 11, $11-x+z$ and 12), are shown here for the sake of clarity.

It is worth noting that the hyperkagome lattice has similarities with the two-dimensional kagome lattice (corner-sharing triangles in two dimensions), which features also four nearest neighbors, as well as with the three-dimensional pyrochlore lattice (corner-sharing tetrahedrons in three dimensions), which could be considered the "mother" crystal structure, featuring six nearest neighbors for each spin. An important property is that all three lattices support dispersionless (flat) one-magnon bands. The shortest closed loop on the hyperkagome lattice beyond the triangles is a decagon; it involves ten bonds. The shortest cycle on the kagome and pyrochlore lattices beyond the triangles is a hexagon; it involves six bonds. Since the even regular polygon (decagon or hexagon) is surrounded by equilateral triangles, one expects a localized-magnon state, which lives on a decagon or hexagon, and belongs to a flat band, for more details see Refs. [48, 49].

In what follows, we examine the thermodynamic properties of model (2) on the hyperkagome lattice over the full temperature range. We also compare our findings to the properties of the two-dimensional kagome-lattice Heisenberg antiferromagnet [50, 51], as well as of the three-dimensional pyrochlore-lattice Heisenberg antiferromagnet [41, 50].

In the remainder of this section, we briefly explain the exploited methods: Numerics for finite-size lattices and high-temperature series complemented with the entropy-method interpolation. Here, we only report the key elements necessary to state our results in Sec. 3.

First, we determine numerically temperature dependencies for periodic lattices of $N = 12$ sites (exact diagonalization) and $N = 24$, 36 sites (finite-temperature Lanczos method); for a similar study of the $S = 1/2$ pyrochlore-lattice Heisenberg antiferromagnet see Refs. [41, 52]. Since the unit cell for the hyperkagome lattice contains 12 sites, finite-lattice numerics is restricted to one unit cell [15] and two or three unit cells arranged as a chain. More details about finite-lattice calculations can be found in Refs. [25, 53, 54]. Our numeric results for finite-size lattices are reported in Figs. 2 and 3 and are discussed in Sec. 3.

Second, we use the high-temperature series expansion up to 16th order, which was reported in Ref. [17] (the Magdeburg HTE code [50, 55] yields the same series of the specific heat and the static uniform susceptibility, however, only up to 13th order), and employ the entropy method [36–38] to obtain temperature dependencies for infinite lattice.

The raw high-temperature series expansion may be improved by simple Padé approximants $[u,d](T) = P_u(\beta)/Q_d(\beta)$. Here, $P_u(\beta)$ and $Q_d(\beta)$ are polynomials of order u and d, $u+d \le 16$, and the series expansion of $[u,d](T)$ coincides with the high-temperature series of c or χ up

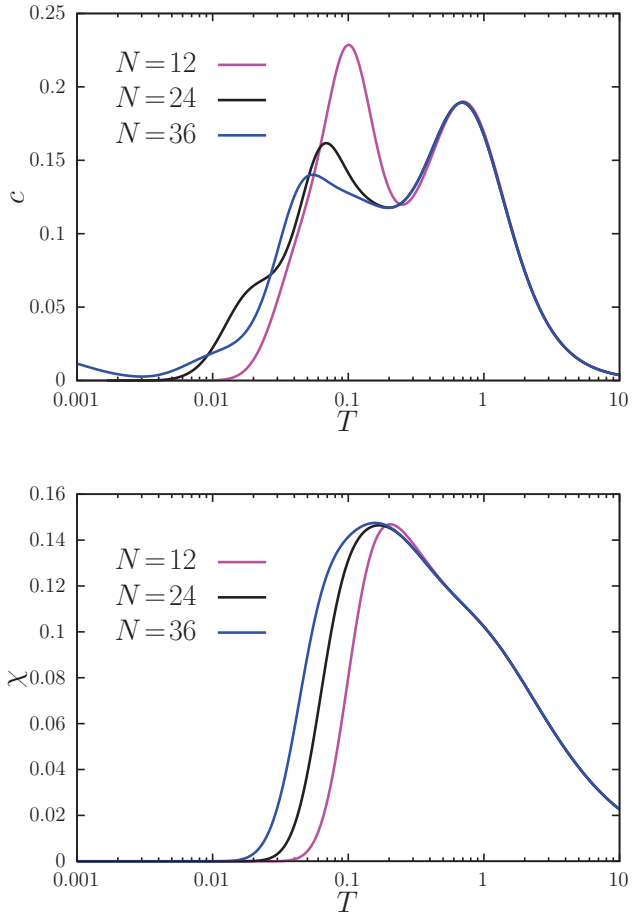

Figure 2. Finite-lattice results for (top) the specific heat and (bottom) the uniform susceptibility. Exact-diagonalization ($N = 12$) and finite-temperature Lanczos method ($N = 24$, number of different random states $R = 200$ [25–27] and $N = 36$, $R = 20$) data. The results for $N = 24$ and $N = 36$ differ from each other below about $T \approx 0.2$.

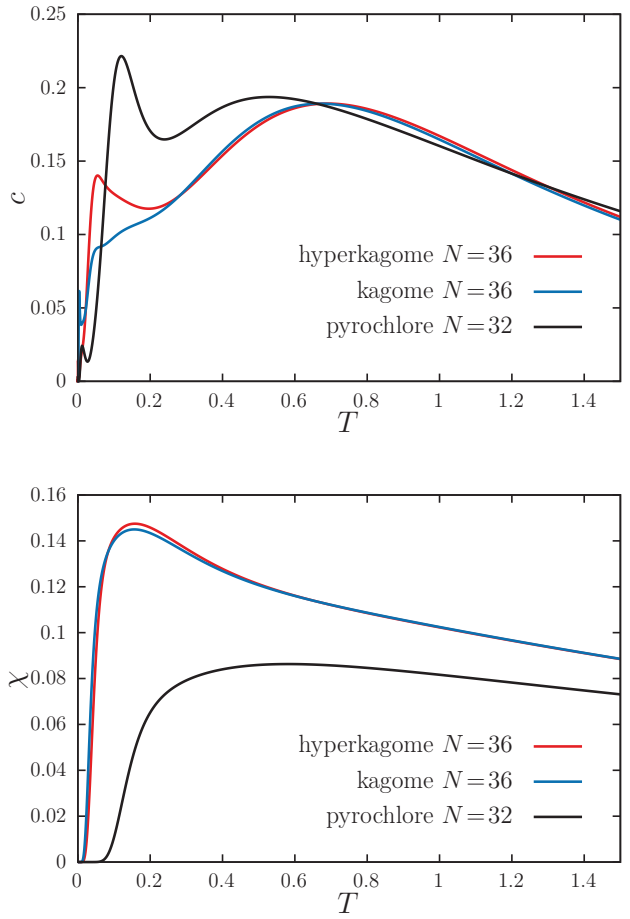

Figure 3. Comparison with the kagome- and pyrochlore-lattice cases for (top) the specific heat and (bottom) the uniform susceptibility. Finite-temperature Lanczos method data for $N = 36$ (hyperkagome lattice, see Fig. 2, and kagome lattice [51]) and $N = 32$ (pyrochlore lattice [41]). The extra low-temperature peak of $c(T)$ at $T \approx 0.117$ for the pyrochlore lattice (top panel, black curve) is a finite-size effect and is not present for $N \to \infty$ [41]. Moreover, the subtle details of $c(T)$ at very low temperatures (top panel) are finite-size effects, too.

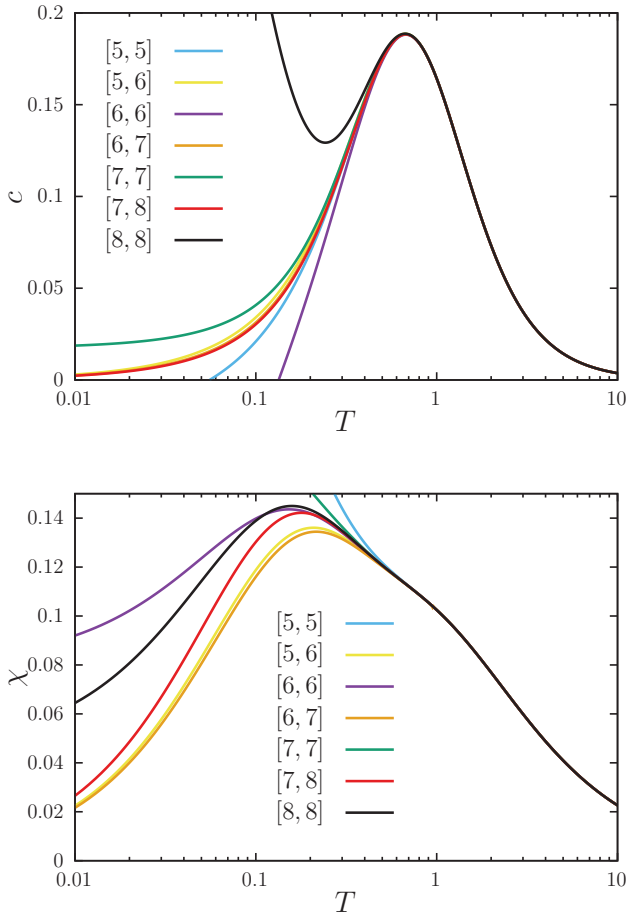

Figure 4. Padé approximants of the high-temperature series [17] for (top) the specific heat and (bottom) the uniform susceptibility. They start to deviate from each other in both panels below $T \approx 0.5$.

to 16th order with respect to $\beta = 1/T$. Comparing close to diagonal Padé approximants in Fig. 4, we conclude that they start to deviate notably one from another below $T \approx 0.5$ and thus can reproduce the high-temperature peak of $c(T)$ at $T \approx 0.669$, but not any of the specific features of $\chi(T)$ since $\chi(T)$ increases monotonously to temperatures well below $T = 0.5$ and also has got its maximum below $T = 0.5$.

In order to study the thermodynamic behavior at lower temperatures we use the entropy-method interpolation scheme introduced by Bernu *et al.* [36–38] and further used in several studies [39–44]. Within the entropy method one interpolates the entropy (per site) s as a function of the mean (internal) energy (per site) e, $s(e)$. As e approaches its maximal value $e_\infty = E(T \to \infty)/N = \mathrm{tr}(H)/N = 0$, the entropy is known from high-temperature series expansion, $s(e) = \ln 2 + \sum_{i>1} a_i e^i$ (i.e., the coefficients $a_2, \ldots, a_{16}$ are known, see Ref. [36]). As e approaches its minimal (ground-state) value e_0, the entropy behaves as $s(e) \propto (e - e_0)^{\alpha/(1+\alpha)}$ if $c(T) = AT^\alpha$ for $T \to 0$ (gapless low-energy excitations) or as $s(e) \propto -[(e - e_0)/\Delta](\ln[\Delta(e - e_0)] - 1)$ if $c(T) \propto e^{-\Delta/T}/T^2$ for $T \to 0$ (gapped low-energy excitations). Next, we interpolate, instead of $s(e)$, an auxiliary function $G(e)$, different for the two types of low-energy excitations, which immediately gives $s(e)$. For the gapless case we have

$$G(e) = \frac{[s(e)]^{\frac{1+\alpha}{\alpha}}}{e - e_0} \to G_{\mathrm{app}}(e) = \frac{(\ln 2)^{\frac{\alpha}{1+\alpha}}}{-e_0} \frac{P_u(e)}{Q_d(e)} \; ;$$
$$s_{\mathrm{app}}(e) = [(e - e_0)\, G_{\mathrm{app}}(e)]^{\frac{\alpha}{1+\alpha}} \; . \qquad (3)$$

And for the gapped case we have

$$G(e) = (e - e_0) \left[\frac{s(e)}{e - e_0}\right]' \to G_{\mathrm{app}}(e) = \frac{\ln 2}{e_0} \frac{P_u(e)}{Q_d(e)} \; ;$$
$$\frac{s_{\mathrm{app}}(e)}{e - e_0} = \frac{\ln 2}{-e_0} - \int_e^0 \mathrm{d}\xi \frac{G_{\mathrm{app}}(\xi)}{\xi - e_0} \; . \qquad (4)$$

Here, $P_u(e)$ and $Q_d(e)$ are the polynomials of order u and d, $u + d \le 16$, and the series expansion of the quotient $[u, d](e) = P_u(e)/Q_d(e)$ coincides with the Maclaurin series of $G(e)$ known up to 16th order. Besides, the prime denotes the derivative with respect to e. Knowing the dependence $s(e)$, we obtain the desired temperature dependence of the specific heat $c(T)$ in parametric form: $T = 1/s'(e)$ and $c = -[s'(e)]^2/s''(e)$. Finally, we can calculate either the prefactor A, $A_{\mathrm{app}} = [\alpha^{1+\alpha}/(1+\alpha)^\alpha][G_{\mathrm{app}}(e_0)]^\alpha$, for the gapless case or the energy gap Δ, $\Delta_{\mathrm{app}} = -1/G_{\mathrm{app}}(e_0)$, for the gapped case. In the presence of a (small) external magnetic field h one

gets the entropy $s_{\rm app}(e,h)$ which yields the uniform susceptibility χ via the relations: $m=[1/s'(e,h)]\partial s(e,h)/\partial h$, $\chi=m/h$ $(h\to 0)$. For further details see Refs. [36, 38, 40, 41, 43].

Thus, to obtain the thermodynamic quantities within the framework of the entropy method one needs, besides the high-temperature series for c and χ, to know i) the ground-state energy e_0, ii) how $c(T)$ vanishes as $T\to 0$, and iii) the value of $\chi_0\equiv\chi(T=0)$ in the case of gapless low-energy excitations. Even if the precise value of e_0 is not available and both gapless and gapped excitations are acceptable, one can proceed as in Ref. [40]. First, one has to assume some reasonable value e_0 in order to explore a certain region of e_0 systematically. Second, one has to assume the exponent α in the case of a gapless spectrum or one has to assume that the spectrum is gapped. Then, for the assumed e_0 and gapless/gapped energy spectrum one has to calculate within the entropy method the specific heat $c(T)$ using all $n_{\rm P}$ available Padé approximants $[u,d](e)$. There are $n+1$ Padé approximants based on the series up to nth order. We discard from the very beginning four Padé approximants $[n,0]$, $[n-1,1]$, $[1,n-1]$, $[0,n]$ so that $n_{\rm P}=n-3$. Next, one has to

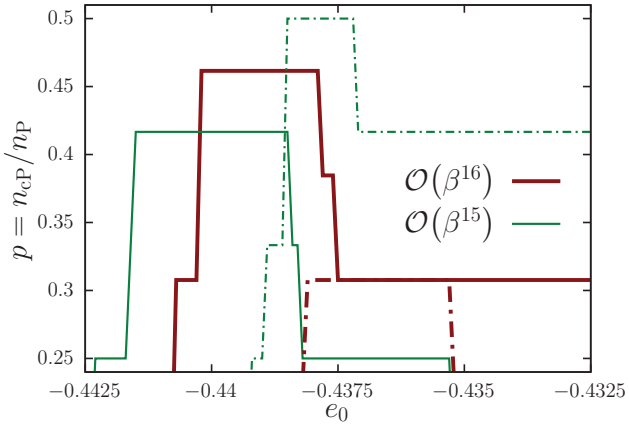

Figure 5. The ratio of the number of "coinciding" entropy-method Padé approximants $n_{\rm cP}$ to the number of all considered entropy-method Padé approximants $n_{\rm P}$, $p=n_{\rm cP}/n_{\rm P}$, based on the series of 15th (thin green) and 16th (thick red) orders as a function of the chosen value of e_0. Here $T_{\rm i}=0.5$, $\Delta T=0.025$, $T_{\rm f}=0.1$, see the main text. We consider both assumptions, gapless (solid) and gapped (dot-dashed) low-energy excitations.

examine the "closeness" of all $n_{\rm P}$ profiles $c(T)$. To this end, we inspect them thoroughly from some high temperature $T_{\rm i}$ down to $T_{\rm f}<T_{\rm i}$ with temperature steps ΔT. If the absolute value of the difference of a certain c from the arithmetic mean value for this bundle, $\overline{c}$, at a running temperature T $(T_{\rm f}\le T\le T_{\rm i})$ is less than, e.g., 0.001, this c belongs to the set of "coinciding" Padé approximants. In the opposite case, this Padé approximant is discarded and not considered for lower temperatures. According to Refs. [40, 43], a large number of coinciding curves $n_{\rm cP}$, or more precisely a large value of $p=n_{\rm cP}/n_{\rm P}$, provides evidence that the assumptions made about e_0 and the low-energy excitations are self-consistent.

In Fig. 5 we illustrate such an analysis based on $n_{\rm P}$ Padé approximants following from the 15th (thin green) and 16th order (thick red) in Eqs. (3) or (4) for the specific heat $c(T)$ under the assumption of a gapless spectrum with $\alpha=2$ (solid) or a gapped spectrum (dot-dashed). Here we set $T_{\rm i}=0.5$, $\Delta T=0.025$, $T_{\rm f}=0.1$. If e_0 is taken in the range $[-0.440\,2,-0.437\,9]$ assuming a gapless spectrum, i.e., $c(T)=AT^2$ as $T\to 0$, and the analysis is based on 16th order ($n_{\rm P}=13$), we find that $n_{\rm cP}=6$ and $p\approx 0.46$. In addition, for the prefactor A we get $A=493{-}727$. If e_0 is taken in the range $-[0.438\,1,-0.435\,3]$ assuming a gapped spectrum and the analysis is based on 16th order, we find $p=4/13\approx 0.31$. In addition, the energy gap is $\Delta=0.025{-}0.018$. All these findings are visualized by the thick red curves in Fig. 5. Slightly different values of e_0 which provide maximal values of p follow from the analysis based on 15th order, see the thin green curves in Fig. 5. Namely, for the gapless spectrum with $e_0\in[-0.441\,5,-0.438\,5]$ we have $p=5/12\approx 0.42$, $A=377{-}563$; for the gapped spectrum with $e_0\in[-0.438\,5,-0.437\,2]$ we have $p=6/12=0.5$, $\Delta=0.027{-}0.024$.

Following the strategy of Refs. [40, 43], we may conclude that the entropy-method prediction for the ground-state energy is $e_0\in[-0.440\,2,-0.437\,9]$ (gapless excitations) or $e_0\in[-0.438\,1,-0.435\,3]$ (gapped excitations). In what follows, we use this missing input parameter e_0 for the entropy method, considering both assumptions about $c(T)$ as $T\to 0$ as well as the minimal and maximal values of e_0 to obtain the light blue and light red shaded areas in Fig. 6. We note in passing that the uniform susceptibility $\chi(T)$ is less convenient for seeking a large value of $p=n_{\rm cP}/n_{\rm P}$, since it requires the additional parameter χ_0 if the spectrum is gapless.

More details about the entropy-method calculations can be found in Refs. [36, 38, 40, 41, 43]. Our entropy-method results are reported in Fig. 6 and are discussed in Sec. 3.

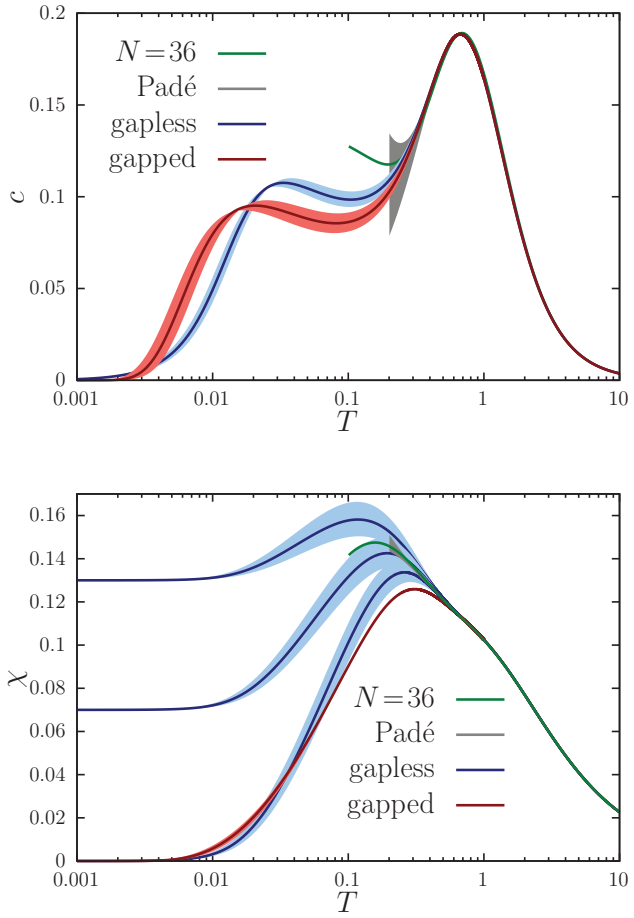

Figure 6. Entropy-method results for (top) the specific heat and (bottom) the uniform susceptibility of the $S = 1/2$ hyperkagome-lattice Heisenberg antiferromagnet. Blue curves correspond to the gapless spectrum ($c = AT^2$ as $T \to 0$) and red ones to the gapped spectrum ($c \propto e^{-\Delta/T}/T^2$ as $T \to 0$). The shaded area (light blue and light red) represents the region of e_0 where p has a maximum (see Fig. 5). We also show $N = 36$ data (green, $T \geq 0.1$) and two simple Padé approximants [7, 7] and [8, 8] for $c(T)$ and $\chi(T)$ and color in gray the region between them ($T \geq 0.2$). In the case of gapless excitations, we examine the three values of χ_0: 0, 0.07, and 0.13.

3. Results

3.1. Ground-state energy e_0

We begin with the discussion of the ground-state energy of the $S = 1/2$ hyperkagome-lattice Heisenberg antiferromagnet. Various proposals about the nature of the ground state, i.e., spin liquids or valence-bond crystals, yield $e_0 \in -[0.430, -0.424]$, see Table 1. Exact diagonalizations for $N = 12, 24, 36$ yield $-0.453\,74$, $-0.446\,33$, $-0.445\,10$, see Table 1, that, apparently, are overestimated values of the thermodynamically large systems. As explained above, to provide consistency of the entropy-method calculations, we have to assume for e_0 the values in $[-0.440, -0.435]$: This is a combination of both possible scenarios of either a gapless or a gapped energy spectrum. Yet another plausible simple approach to determine e_0 from the high-temperature series expansion [6] yields e_0 about -0.448. The determination of e_0 based on the high-temperature series expansion seems to be rather formal, since it does not use any specific picture for the ground state. However, the experience from other models, including exactly solvable ones and precisely examined numerically ones, gives hints that it may yield quite reasonable predictions [40, 43].

It is worth noting that the ground-state energy for the kagome lattice is quite close: $-0.438\,6(5)$ [56, 57], $-0.438\,7$ [58] (i.e., about -0.219 per bond), but for the pyrochlore lattice it is rather different: $-0.490(6)$ [6], $-0.483\,1(1)$ [7], -0.489 [9] (i.e., about -0.163 per bond).

3.2. Thermodynamic properties

We pass to the finite-temperature properties of the $S = 1/2$ hyperkagome-lattice Heisenberg antiferromagnet. First, in Figs. 2 and 3 we report the temperature dependence of the specific heat $c(T)$ and the uniform susceptibility $\chi(T)$ obtained for finite lattices of $N = 12$, 24, 36.

Table 1. Ground-state energy e_0 obtained by different authors

N=12 [15]	-0.454
N=12/24/36 (present paper)	$-0.453\,74/-0.446\,33/-0.445\,10$
QSL [15]	-0.424
VBC [16]	$-0.430\,115$
EM (present paper)	$[-0.440, -0.435]$

Second, in Fig. 6 we report $c(T)$ and $\chi(T)$ obtained by the entropy method. Here, both possibilities, the gapless spectrum with $\alpha = 2$ or the gapped spectrum, were considered, see blue and red curves, respectively. The ground-state energy e_0 was determined from the analysis of $c(T)$ as was explained in Sec. 2. We used $[8, 8](e)$ in Eqs. (3) or (4) as well as the region of e_0 where p has a maximum, see Fig. 5, in order to estimate the spread of the derived functions. For the gapless excitations we set $\chi_0 = 0$, 0.07, 0.13.

Let us now discuss the thermodynamic quantities of the $S = 1/2$ hyperkagome-lattice Heisenberg antiferromagnet in some detail. As it follows from the upper panel of Fig. 2, the high-temperature peak of the specific heat does not show any finite-size scaling; it is already provided by the calculations for one unit cell ($N = 12$). On these grounds, we thus speculate that the curve of the specific heat at temperatures of the high-temperature peak and above represents the thermodynamic limit[2], see also $N = 36$ data in Fig. 6. The position of the low-temperature peak, on the other hand, does depend on the size; it is at $T \approx 0.101$ for $N = 12$, at $T \approx 0.069$ for $N = 24$, and at $T \approx 0.055$ for $N = 36$. Moreover, the height decreases notably with growing N. The results of the entropy method in Fig. 6 refer to the infinite lattice. As it follows from Fig. 6, the specific heat $c(T)$ besides the high-temperature peak at $T \approx 0.669$ has an additional low-temperature one at about $T \approx 0.033$ (gapless excitations) or $T \approx 0.021$ (gapped excitations); the height of the low-temperature peak is about two times smaller than the height of the main peak.

As can be seen in the lower panel of Fig. 2, the maximum of $\chi(T)$ has a mild dependence on system size; it occurs at $T \approx 0.204$ for $N = 12$, at $T \approx 0.168$ for $N = 24$, and at $T \approx 0.158$ for $N = 36$. Moreover, the height remains practically unchanged. This behavior can be traced back to the size of the singlet-triplet gap for these systems. Its value is $\Delta_{\mathrm{s-t}} \approx 0.383, 0.216, 0.136$ for $N = 12, 24, 36$, respectively. According to the entropy-method analysis reported in Fig. 6, the uniform susceptibility $\chi(T)$ behaves identically at T above about 0.5 for gapless and gapped excitations. For lower temperatures, $\chi(T)$ has a maximum at $T \approx 0.118$ if $\chi_0 = 0.13$, at $T \approx 0.194$ if $\chi_0 = 0.07$, at $T \approx 0.260$ if $\chi_0 = 0$ (gapless excitations) or at $T \approx 0.309$ (gapped excitations) and then smoothly approaches χ_0 as the temperature goes to zero.

[2]In contrast, the results for the $S = 1/2$ pyrochlore-lattice Heisenberg antiferromagnet of $N = 32$ sites [41] reflect the thermodynamic limit only for $T > 0.7$, well above the temperature of the high-temperature peak of $c(T)$. Therefore, the finite-lattice results for the hyperkagome case allow a reliable discussion of thermodynamic properties for much lower temperatures down to $T \approx 0.2$.

An important general message that can be taken from Fig. 6 is that the entropy-method and finite-system numerical data (and even simple Padé approximants for χ) favour the assumption of a gapless spectrum with finite χ_0 around 0.1.

It is worthy to put our results for the hyperkagome lattice in the context of prior work for the kagome and pyrochlore lattices. Concerning $c(T)$ (the upper panels of Figs. 2 and 6), its features at least at intermediate temperatures and above, are quite similar to what is known for the kagome-lattice and also the square-kagome-lattice case (a peak at $T = 0.67$, a shoulder of two times smaller height at $T = 0.1-0.25$ [51, 59]), but differ from those for the pyrochlore-lattice case, where only one maximum in $c(T)$, but no additional low-temperature feature such as peak or shoulder was found [41, 60]. Concerning $\chi(T)$ (the lower panels of Figs. 2 and 6), it resembles the maximum of $\chi(T)$ for the finite-size kagome lattices [51] and for the infinite kagome lattice analyzed by the entropy method [38]. In contrast, for the pyrochlore lattice we have several scenarios, none of which can be excluded to date [41, 60, 61].

To further discuss similarities between the hyperkagome-lattice Heisenberg antiferromagnet and the kagome-lattice one and differences to the pyrochlore-lattice one, we compare in Fig. 3 the finite-temperature Lanczos method data for $c(T)$ and $\chi(T)$ for the hyperkagome-lattice case with the kagome-lattice and pyrochlore-lattice cases. We have to remark here that the energy scale is different for the pyrochlore (each site has six neighbors) and the kagome or hyperkagome (each site has four neighbors) and one may rescale $T \to T/z$ and $\chi \to \chi z$ so that different lattices, with $z = 4$ and $z = 6$, can be compared, but the conclusions below remain unchanged. Namely, Fig. 3 illustrates a good agreement above about $T = 0.25$ for the specific heat (top panel) and even for all temperatures for the uniform susceptibility (bottom panel) for the hyperkagome-lattice and kagome-lattice Heisenberg antiferromagnets. In contrast, the pyrochlore-lattice Heisenberg antiferromagnet shows different temperature profiles $c(T)$ and $\chi(T)$, also after rescaling. Thus, we may conclude that the three-dimensional hyperkagome lattice is closer to highly frustrated two-dimensional lattices (kagome, square-kagome) than to the three-dimensional pyrochlore lattice. However, it is worth noting the difference: For the kagome lattice the low-temperature peak of $c(T)$ moves to higher temperatures with increasing N [51], opposite to what is observed for the hyperkagome lattice (recall the top panel of Fig. 2). Thus, for the kagome lattice one yields a low-temperature shoulder of the main peak in the thermodynamic limit [62].

High-temperature series expansions offer important insight into simi-

larities and differences between the hyperkagome-lattice, kagome-lattice and pyrochlore-lattice cases. The high-temperature series expansions for c coincide for the hyperkagome and kagome lattices up to β^5, but differ for the pyrochlore lattice already in terms proportional to β^2. Likewise, the high-temperature series expansions for χ coincide for the hyperkagome-lattice and kagome-lattice cases up to β^6, but differ for the pyrochlore-lattice case already in terms proportional to β^3. Such distinctness in high-energy processes can be traced back to the building blocks of these lattices (triangle for hyperkagome and kagome, but tetrahedron for pyrochlore) and shortest closed loops beyond, i.e., decagon for hyperkagome and hexagon for kagome and pyrochlore.

4. Summary and outlook

In the present paper, we consider the $S = 1/2$ hyperkagome-lattice Heisenberg antiferromagnet – a benchmark frustrated quantum spin-lattice model. Using finite-lattice calculations and high-temperature series expansion up to 16th order [17] complemented by plausible assumptions about low-temperature properties we have obtained the temperature dependence for the specific heat and the uniform susceptibility, see Figs. 2 and 6. Our main findings are as follows: We observe a two-peak profile for $c(T)$ at $T \approx 0.021{-}0.033$ and $T \approx 0.669$, and find evidence in favour of gapless excitations which implies the maximum of $\chi(T)$ at $T \approx 0.118{-}0.194$ and finite χ at $T = 0$ around 0.1. As a byproduct, we can restrict the ground-state energy to $e_0 \in [-0.440, -0.435]$, which provides self-consistency of the entropy-method calculations. We have found that the thermodynamics of the three-dimensional hyperkagome-lattice Heisenberg antiferromagnet is quite similar to the two-dimensional kagome-lattice one, but differs from that of the pyrochlore lattice.

Future work on thermodynamics may be related to application of universal and specific tools to tackle the problem. Evidently, the $S = 1/2$ hyperkagome-lattice Heisenberg antiferromagnet can be studied by the rotation-invariant Green's function method for obtaining approximate thermodynamic and dynamic quantities on an equal footing. Similar studies for the quantum kagome-lattice and pyrochlore-lattice Heisenberg antiferomagnets were reported in Refs. [34, 35]. Moreover, the hyperkagome-lattice Heisenberg antiferromagnet represents a flat-band system, since the one-magnon energy spectrum has dispersionless (flat) bands. The flat-band states may be relevant at high fields and low temperatures and their dominant contribution to thermodynamics can be elaborated by special methods of flat-band systems, see Refs. [48, 49].

Acknowledgements

T. H. was supported by the fellowship of the President of Ukraine for young scholars and by the Projects of research works of young scientists of the National Academy of Sciences of Ukraine (project # 29-04/18-2023, Frustrated quantum magnets at finite temperatures). O. D. thanks J. Strečka for the kind hospitality at the MECO48 conference (Stará Lesná, Slovakia, May 22–26, 2023). O. D. acknowledges the kind hospitality of the University of Bielefeld in October-December of 2023 (supported by Erasmus+ and DFG). This work was supported by the Deutsche Forschungsgemeinschaft (DFG SCHN 615/28-1 and RI 615/25-1).

References

1. C. Berthier, L. P. Lévy, and G. Martinez, eds., *High Magnetic Fields: Applications in Condensed Matter Physics and Spectroscopy*, Vol. 595 (Springer Berlin, Heidelberg, 2002).
2. U. Schollwöck, J. Richter, D. J. J. Farnell, and R. F. Bishop, eds., *Quantum Magnetism*, Vol. 645 (Springer Berlin, Heidelberg, 2004).
3. H. T. Diep, ed., *Frustrated Spin Systems* (World Scientific, Singapore, 2005).
4. C. Lacroix, P. Mendels, and F. Mila, *Introduction to Frustrated Magnetism – Materials, Experiments, Theory*, Springer Series in Solid-State Sciences, Vol. 164 (Springer, Berlin, Heidelberg, 2011).
5. B. Canals and C. Lacroix, Phys. Rev. Lett. **80**, 2933 (1998).
6. I. Hagymási, R. Schäfer, R. Moessner, and D. J. Luitz, Phys. Rev. Lett. **126**, 117204 (2021).
7. N. Astrakhantsev, T. Westerhout, A. Tiwari, K. Choo, A. Chen, M. H. Fischer, G. Carleo, and T. Neupert, Phys. Rev. X **11**, 041021 (2021).
8. M. Hering, V. Noculak, F. Ferrari, Y. Iqbal, and J. Reuther, Phys. Rev. B **105**, 054426 (2022).
9. R. Schäfer, B. Placke, O. Benton, and R. Moessner, Phys. Rev. Lett. **131**, 096702 (2023).
10. Y. Okamoto, M. Nohara, H. Aruga-Katori, and H. Takagi, Phys. Rev. Lett. **99**, 137207 (2007).
11. J. M. Hopkinson, S. V. Isakov, H.-Y. Kee, and Y. B. Kim, Phys. Rev. Lett. **99**, 037201 (2007).
12. M. J. Lawler, H.-Y. Kee, Y. B. Kim, and A. Vishwanath, Phys. Rev. Lett. **100**, 227201 (2008).

13. M. E. Zhitomirsky, Phys. Rev. B **78**, 094423 (2008).
14. Y. Zhou, P. A. Lee, T.-K. Ng, and F.-C. Zhang, Phys. Rev. Lett. **101**, 197201 (2008).
15. M. J. Lawler, A. Paramekanti, Y. B. Kim, and L. Balents, Phys. Rev. Lett. **101**, 197202 (2008).
16. E. J. Bergholtz, A. M. Läuchli, and R. Moessner, Phys. Rev. Lett. **105**, 237202 (2010).
17. R. R. P. Singh and J. Oitmaa, Phys. Rev. B **85**, 104406 (2012).
18. Y. Wan and Y. B. Kim, Phys. Rev. B **94**, 224401 (2016).
19. F. L. Buessen and S. Trebst, Phys. Rev. B **94**, 235138 (2016).
20. B. Koteswararao, R. Kumar, P. Khuntia, S. Bhowal, S. K. Panda, M. R. Rahman, A. V. Mahajan, I. Dasgupta, M. Baenitz, K. H. Kim, and F. C. Chou, Phys. Rev. B **90**, 035141 (2014).
21. S. Chillal, Y. Iqbal, H. O. Jeschke, J. A. Rodriguez-Rivera, R. Bewley, P. Manuel, D. Khalyavin, P. Steffens, R. Thomale, A. T. M. N. Islam, J. Reuther, and B. Lake, Nature Communications **11**, 2348 (2020).
22. B. Sana, M. Barik, M. Pregelj, U. Jena, M. Baenitz, J. Sichelschmidt, K. Sethupathi, and P. Khuntia, Phys. Rev. B **108**, 134413 (2023).
23. B. Huang, Y. B. Kim, and Y.-M. Lu, Phys. Rev. B **95**, 054404 (2017).
24. P. Henelius and A. W. Sandvik, Phys. Rev. B **62**, 1102 (2000).
25. J. Jaklič and P. Prelovšek, Phys. Rev. B **49**, 5065 (1994).
26. R. Schnalle and J. Schnack, Int. Rev. Phys. Chem. **29**, 403 (2010).
27. J. Schnack, J. Richter, and R. Steinigeweg, Phys. Rev. Research **2**, 013186 (2020).
28. J. Ummethum, J. Schnack, and A. Läuchli, J. Magn. Magn. Mater. **327**, 103 (2013).
29. P. M. Richards, Phys. Rev. Lett. **27**, 1800 (1971).
30. J. Kondo and K. Yamaji, Prog. Theor. Phys. **47**, 807 (1972).
31. H. Shimahara and S. Takada, J. Phys. Soc. Jpn. **60**, 2394 (1991).
32. A. F. Barabanov and V. M. Beresovsky, J. Phys. Soc. Jpn. **63**, 3974 (1994).
33. S. Winterfeldt and D. Ihle, Phys. Rev. B **56**, 5535 (1997).
34. P. Müller, A. Zander, and J. Richter, Phys. Rev. B **98**, 024414 (2018).
35. P. Müller, A. Lohmann, J. Richter, and O. Derzhko, Phys. Rev. B **100**, 024424 (2019).
36. B. Bernu and G. Misguich, Phys. Rev. B **63**, 134409 (2001).
37. G. Misguich and B. Bernu, Phys. Rev. B **71**, 014417 (2005).
38. B. Bernu and C. Lhuillier, Phys. Rev. Lett. **114**, 057201 (2015).
39. H.-J. Schmidt, A. Hauser, A. Lohmann, and J. Richter, Phys. Rev. E **95**, 042110 (2017).

40. B. Bernu, L. Pierre, K. Essafi, and L. Messio, Phys. Rev. B **101**, 140403 (2020).
41. O. Derzhko, T. Hutak, T. Krokhmalskii, J. Schnack, and J. Richter, Phys. Rev. B **101**, 174426 (2020).
42. V. Grison, P. Viot, B. Bernu, and L. Messio, Phys. Rev. B **102**, 214424 (2020).
43. M. G. Gonzalez, B. Bernu, L. Pierre, and L. Messio, SciPost Phys. **12**, 112 (2022).
44. T. Hutak, T. Krokhmalskii, O. Derzhko, and J. Richter, Eur. Phys. J. B **96**, 50 (2023).
45. H.-K. Jin and Y. Zhou, Phys. Rev. B **101**, 054408 (2020).
46. L. E. Chern and Y. B. Kim, Phys. Rev. B **104**, 094413 (2021).
47. R. Pohle and L. D. C. Jaubert, Phys. Rev. B **108**, 024411 (2023).
48. O. Derzhko, J. Richter, A. Honecker, and H.-J. Schmidt, Low Temp. Phys. **33**, 745 (2007).
49. O. Derzhko, J. Richter, and M. Maksymenko, Int. J. Mod. Phys. B **29**, 1530007 (2015).
50. A. Lohmann, H.-J. Schmidt, and J. Richter, Phys. Rev. B **89**, 014415 (2014).
51. J. Schnack, J. Schulenburg, and J. Richter, Phys. Rev. B **98**, 094423 (2018).
52. V. R. Chandra and J. Sahoo, Phys. Rev. B **97**, 144407 (2018).
53. J. Schulenburg, *spinpack 2.58*, Magdeburg University (2019).
54. J. Richter and J. Schulenburg, Eur. Phys. J. B **73**, 117 (2010).
55. H.-J. Schmidt, A. Lohmann, and J. Richter, Phys. Rev. B **84**, 104443 (2011).
56. S. Yan, D. A. Huse, and S. R. White, Science **332**, 1173 (2011).
57. S. Depenbrock, I. P. McCulloch, and U. Schollwöck, Phys. Rev. Lett. **109**, 067201 (2012).
58. A. M. Läuchli, J. Sudan, and R. Moessner, Phys. Rev. B **100**, 155142 (2019).
59. J. Richter, O. Derzhko, and J. Schnack, Phys. Rev. B **105**, 144427 (2022).
60. R. Schäfer, I. Hagymási, R. Moessner, and D. J. Luitz, Phys. Rev. B **102**, 054408 (2020).
61. Y. Huang, K. Chen, Y. Deng, N. Prokof'ev, and B. Svistunov, Phys. Rev. Lett. **116**, 177203 (2016).
62. X. Chen, S.-J. Ran, T. Liu, C. Peng, Y.-Z. Huang, and G. Su, Science Bulletin **63**, 1545 (2018).

CONDENSED MATTER PHYSICS

The journal **Condensed Matter Physics** is founded in 1993 and published by Institute for Condensed Matter Physics of the National Academy of Sciences of Ukraine.

AIMS AND SCOPE: The journal **Condensed Matter Physics** contains research and review articles in the field of statistical mechanics and condensed matter theory. The main attention is paid to physics of solid, liquid and amorphous systems, phase equilibria and phase transitions, thermal, structural, electric, magnetic and optical properties of condensed matter. Condensed Matter Physics is published quarterly.

ABSTRACTED/INDEXED IN: Chemical Abstract Service, Current Contents/Physical, Chemical&Earth Sciences; ISI Science Citation Index-Expanded, ISI Alerting Services; INSPEC; "Referatyvnyj Zhurnal"; "Dzherelo".

CONTACT INFORMATION:
Institute for Condensed Matter Physics
of the National Academy of Sciences of Ukraine
1 Svientsitskii Str., 79011 Lviv, Ukraine
Tel: +38(032)2761978; Fax: +38(032)2761158
E-mail: cmp@icmp.lviv.ua http://www.icmp.lviv.ua